Experimental and *ab initio* molecular dynamics simulation studies of liquid $Al_{60}Cu_{40}$ alloy

S. Y. Wang,[1,2] M. J. Kramer,[2] M. Xu,[1] S. Wu,[1] S. G. Hao,[2] D. J. Sordelet,[2] K. M. Ho,[2,3] and C. Z. Wang[2,3]
[1]*Department of Optical Science and Engineering, State Key Laboratory for Advanced Photonic Materials and Devices, Fudan University, Shanghai 200433, People's Republic of China*
[2]*Materials Science and Engineering, Ames Laboratory (USDOE), Ames, Iowa 50011, USA*
[3]*Department of Physics and Astronomy, Iowa State University, Ames, Iowa 50011, USA*
(Received 8 November 2008; revised manuscript received 14 March 2009; published 17 April 2009)

X-ray diffraction and *ab initio* molecular dynamics simulation studies of molten $Al_{60}Cu_{40}$ have been carried out between 973 and 1323 K. The structures obtained from our simulated atomic models are fully consistent with the experimental results. The local structures of the models analyzed using Honeycutt-Andersen and Voronoi tessellation methods clearly demonstrate that as the temperatures of the liquid is lowered it becomes more ordered. While no one cluster-type dominates the local structure of this liquid, the most prevalent polyhedra in the liquid structure can be described as distorted icosahedra. No obvious correlations between the clusters observed in the liquid and known stable crystalline phases in this system were observed.

DOI: 10.1103/PhysRevB.79.144205 PACS number(s): 61.20.Ja, 61.05.C−, 61.25.Mv

I. INTRODUCTION

Solidification of crystalline phases from the liquid is a highly complex, yet critically important process involving phase selection and growth that is of academic interest and also has many practical considerations.[1] In order to fully model this process at the atomic level, we must begin with an accurate description of the local atomic structure of the liquid and further describe how it changes as a function of temperature. Accurately describing the liquid state is complicated by its lack of long-range order and the inherently statistical nature of its short-range order (SRO). However, the local atomic arrangement of the nearest neighbors is expected to play an important role in the properties of liquid and amorphous materials.[2–4] Recently, *ab initio* molecular dynamics (MD) simulations of the amorphous solids and liquid have provided profound insights into the structures and properties of these disordered materials, especially when the calculated data closely correspond to the experimental data. The consistency between the computer simulation and experimental data lends strong support to the further analysis of the structural and electronic properties of the amorphous or liquid systems.

In this paper liquid structures of an $Al_{60}Cu_{40}$ alloy throughout a 450 K span of superheat temperature are studied both by experiments and *ab initio* MD simulations. The theoretical atomic configurations of the liquid structures are verified by comparing the calculated pair-correlation functions with the experimental results. The atomic configurations derived are further investigated using standard geometric methods. The local atomic structure of the liquid is then compared to various crystalline phases reported for Al-Cu alloys to check for topological similarities.

II. EXPERIMENTAL AND SIMULATION DETAILS

The molten alloys with the composition of $Al_{60}Cu_{40}$ are investigated at eight temperatures, 973, 1023, 1073, 1123, 1173, 1223, 1273, and 1323 K, using high-energy synchrotron x-ray diffraction (HEXRD). The melting point of this alloy is about 933 K. In order to obtain the diffraction data, $Al_{60}Cu_{40}$ samples, which were cast from appropriate mixtures of high-purity Al (99.999%) and Cu (99.999%), were sealed in thin-walled 1×2 mm diameter quartz channels and sealed in $\approx$6.7 MPa ($\approx$500 torr) Ar. The samples were uniformly heated using a cylindrical Pt-Rh wound resistance furnace, which has a very low-temperature gradient.[5] We observed that the samples could be heated to $\approx$1400 K before reaction with the container occurred. The HEXRD studies were performed at the MUCAT 6-IDD beamline at the Advanced Photon Source using an energy of 97.84 keV, corresponding to a wavelength (λ) of 0.126 43 Å. Silicon double-crystal monochrometers were employed to select the wavelength. The diffraction data were collected in transmission using a MAR345 image plate detector at a distance around 0.425 m providing a usable range in the wave momentum number ($q=4\pi \sin\theta/\lambda$) of 0.7–17.7 $Å^{-1}$. The diffracted intensity as a function of q was obtained by integrating around the Debye rings of the exposed image plate. The wavelength was determined using an energy dispersive detector while the sample to detector distance was determined using NIST Si Standard Reference Material 640C. The required geometric corrections for misalignment of the detector relative to the beam normal were performed using FIT2D.[6] The data were then converted to the total structure function, $S(q)$, using standard procedures.[7,8] An acquisition time of 200 s provides high quality data with signal to noise comparable to neutron data sets whose acquisition times are 1 to 2 orders of magnitude longer in duration.[9]

The computational models of $Al_{60}Cu_{40}$ are carried out by *ab initio* MD simulations, performed using the VASP code combined with canonical NVT ensembles,[10] and the temperature is controlled using the Nosé-Hoover thermostat.[11,12] The Vanderbilt-type ultrasoft pseudopotentials and the local-density approximation (LDA) are applied in our simulations, and only Γ point is considered for sampling the Brillouin zone of the supercell used in the simulations. 100 atoms consisting of 60 Al and 40 Cu are initially put by random in a cubic box and heated up to 2000 K in order to remove the memory effects from the initial configuration. Then the system is cooled down to the designated temperatures and sta-

bilized for 3000 time steps (3 fs/step). The atomic number density ρ_0 at each temperature is initially calculated from the linear combination of the densities of pure ρ_{Al} and ρ_{Cu} at the corresponding temperature, i.e., $\rho_0=0.6\rho_{Al}+0.4\rho_{Cu}$, using the mass density of $d(t)=a-b(t-t_M)$ for Al from Crawley,[13] where $a=2.375$ gcm^{-3}, $b=0.000\,233$ g cm^{-3} °C^{-1}, and t_M is the melting temperature of pure Al equals to 660.32 °C, the mass density for Cu equals to 8.02 gcm^{-3}, which is the density at the melting temperature of 1084.62 °C. The atomic number density of the sample was then adjusted during the MD simulation by approximately keeping internal pressure essentially zero. The optimized atomic number densities are 0.062 49, 0.0624, 0.062 24, 0.062 07, 0.061 88, 0.061 69, 0.061 44, and 0.061 26 atom/Å^3, respectively, for the liquid at temperatures of 973, 1023, 1073, 1123, 1173, 1223, 1273, and 1323 K. The corresponding simulation cell of 100 atoms in a cubic box has the box length of 11.696 84, 11.702 59, 11.712 59, 11.722 96, 11.734 86, 11.746 77, 11.762 64, 11.774 55 Å, respectively.

The experimental pair-correlation function (PCF), $g(r)$, is obtained by Fourier transformation of the measured total structure factor $S(q)$ using the following equation:

$$g(r)=\frac{\rho(r)}{\rho_o}=1+\frac{1}{4\pi r\rho_o}\left[\frac{2}{\pi}\int_0^\infty q[S(q)-1]\sin(qr)dq\right], \tag{1}$$

where $\rho(r)$ is the atomic density at a distance r from an average atom located at the origin, and ρ_0 is the average atomic density of the material.

From the atomic coordinates generated by the *ab initio* MD, the theoretical partial PCF $g_{\alpha\beta}(r)$ between the atom type α and β can be calculated,

$$g_{\alpha\beta}(r)=\rho_{\alpha\beta}^{-2}\left\langle\sum_i\sum_{j\neq i}\delta(\vec{r}_{i\alpha})\delta(\vec{r}_{j\beta}-r)\right\rangle, \tag{2}$$

where $\rho_{\alpha\beta}=\rho_0\sqrt{a_\alpha a_\beta}$ corresponding partial density with ρ_0 being the atomic density of the liquid and a_α and a_β being the atomic concentration of the corresponding elements in the liquid.

The calculated total structure factor $S(q)$ from the simulations were obtained using the Faber-Ziman formalism[14] from the three partial structure factors $S_{\alpha\beta}(q)$, atomic concentration of the elements a_α and a_β and the scattering factors f_α and f_β in the alloys,

$$S(q)-1=\frac{a_\alpha^2 f_\alpha^2[S_{\alpha\alpha}(q)-1]+2a_\alpha a_\beta f_\alpha f_\beta[S_{\alpha\beta}(q)-1]+a_\beta^2 f_\beta^2[S_{\beta\beta}(q)-1]}{(a_\alpha f_\alpha+a_\beta f_\beta)^2}. \tag{3}$$

The scattering factors f_α and f_β are obtained from tabulated data.[15] The partial structure factors, $S_{\alpha\beta}(q)$, are related to the partial pair-correlation functions $g_{\alpha\beta}(r)$ by

$$S_{\alpha\beta}(q)=\delta_{\alpha\beta}+4\pi\rho_{\alpha\beta}\int_0^\infty[g_{\alpha\beta}(r)-1]\frac{\sin(qr)}{qr}r^2dr, \tag{4}$$

where the $g_{\alpha\beta}(r)$ can be calculated by Eq. (2). We note that besides the Faber-Ziman partial structure factors, there are also other two different sets of partial structure factors proposed in the literature for analyzing the local ordering of the binary alloy, i.e., the Ashcroft-Langreth[16] and the Bathia-Thornton[17] partial structure factors. The relations between the three different sets of partial structure factors have been given in the book by Waseda.[18]

The total pair-correlation function, $g(r)$, from the *ab initio* MD simulation can then be calculated by the Fourier transformation of structure factor $S(q)$ using the standard transformation techniques as described by Eq. (1).

While the interatomic forces from the VASP code are accurate, the quantum mechanics calculations require very heavy computation and large memory space and *ab initio* MD simulation is usually limited to a few hundred atoms and with simulation time of tens of picoseconds. Therefore, caution should be taken when interpreting the results obtained from the *ab initio* MD simulations. In general, as long as the spatial correlation length of the system being studied is less than $\frac{1}{2}$ of the box length of the MD cell and the dynamics of the system is much faster than the MD simulation time, such as the liquid state we studied in this paper, the results from *ab initio* MD simulations should be reliable. We have carefully examined the convergence of our results with respect to the size and time used in our simulation. We find the structural properties obtained from the simulation using the 100-atom and 200-atom unit cell are very similar (see Sec. III). Moreover, statistical average over 6 and 9 ps also gives a very similar result for the structural properties. The diffusion constant is more sensitive to the box size than the structural properties, but it should be about ~10% of errors.

III. RESULTS AND DISCUSSION

A. Structure factor and the pair-correlation functions

Figure 1 illustrates the total structure factor $S(q)$ of the liquid $Al_{60}Cu_{40}$ alloy as the function of the temperatures between 973 and 1323 K at 50 K intervals obtained from our HEXRD experiments. The first peaks of the $S(q)$ are located around 3.01 Å^{-1}, and the amplitudes of the first peak are reduced with increasing the temperature. The second peak, spanning from ~4.2 to 6.6 Å^{-1}, is asymmetric with the asymmetry decreasing with increasing temperature. The experimental and calculated total $g(r)$ functions obtained from Eqs. (1) and (2) respectively, are shown in Fig. 2(a). The first

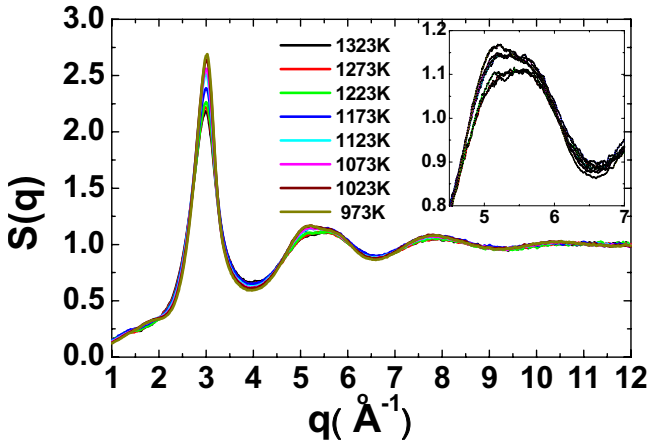

FIG. 1. (Color online) Experimental total structure factor $S(q)$ of the liquid $Al_{60}Cu_{40}$ alloy at different temperatures. Inset shows the details of the second diffuse scattering peak.

peak of the $g(r)$ is around 2.58 Å, and its height decreases with increasing the temperature. The second and the third peaks are located around 4.54 and 6.72 Å, respectively. The locations of the peaks and valleys of the PCF curves shift less than 0.2 Å over this temperature range. The simulated results of the total correlation functions agree remarkably well with the experiments for all temperatures, especially

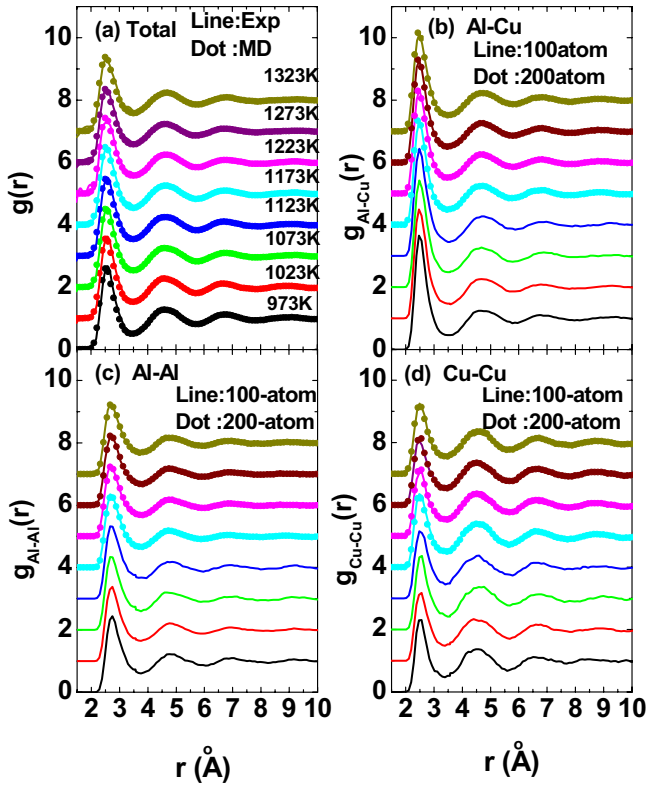

FIG. 2. (Color online) The total and partial pair-correlation functions $g(r)$ of the liquid $Al_{60}Cu_{40}$ alloy at different temperature. The experimental data transformed to the PCF using Eq. (1) are shown as lines in (a), the partial pair-correlation functions $g(r)$ of the liquid $Al_{60}Cu_{40}$ alloy at four different temperatures using two different supercells are shown in (b), (c), and (d).

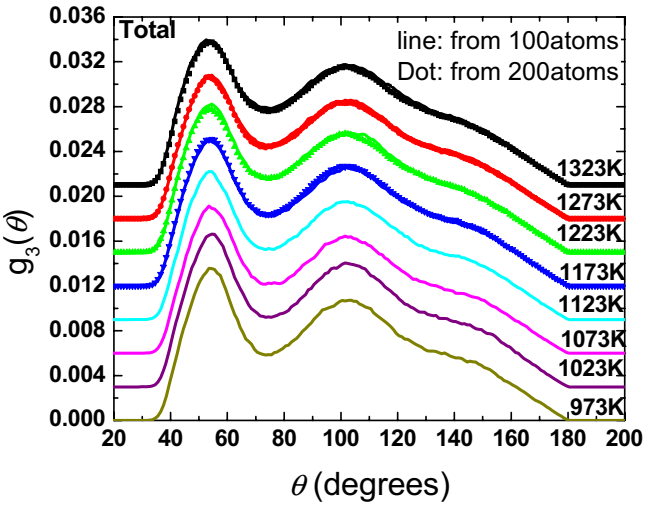

FIG. 3. (Color online) Bond-angle distribution functions of the liquid $Al_{60}Cu_{40}$ alloy at different temperatures, The data got from two different supercells at four different temperatures are also shown as dot.

both the locations and the amplitudes of their peaks, providing strong support for accuracy liquid structure using our *ab initio* MD method.

The partial correlation functions, which are calculated from the theoretical model, are also shown in Figs. 2(b)–2(d), respectively. The first peaks of the partial correlation functions are centered at 2.67, 2.48, and 2.56 Å, respectively, for g_{Al-Al}, g_{Al-Cu}, and g_{Cu-Cu} pairs, and the locations of these peaks are almost invariant with the temperature. The second peaks are centered at 4.76, 4.66, and 4.55 Å for Al-Al, Al-Cu, and Cu-Cu pairs. The lack of periodicity in the separation of the position of each of the peaks for the partial pairs in real space will result in asymmetric and broader second peaks of the total structure factor in Fig. 1. From the partial correlation function the distances between Al-Al pairs are the longest, so it is assumed that the higher proportion of Al atoms in a cluster the larger that cluster must be. In addition, the amplitude of the first peaks of g_{Al-Cu} is higher than the others, indicating that the interaction between Al-Cu is stronger than Al-Al or Cu-Cu.

B. Local structure analysis based on the MD models

A metric for the local structure of the liquid system is its bond-angle distribution function, $g_3(\theta)$, which is defined for the angles between the nearest neighboring atoms around a central atom within the maximum bond length defined by R_{cut}. Using the bond-length cutoff of 3.56 Å, which is the first minimum in the pair-correlation functions, the total bond-angle distribution functions of the liquid $Al_{60}Cu_{40}$ alloy at different temperatures are calculated and shown in Fig. 3. The first prominent peak of the function is located at an angle of about 54.5° and the second one is near 104.5°. The peaks are more pronounced at lower temperatures, indicating that the distribution of the local structure types decreases at lower temperatures. The shoulders that appear at 150°, which become more pronounced as the temperature is decreased,

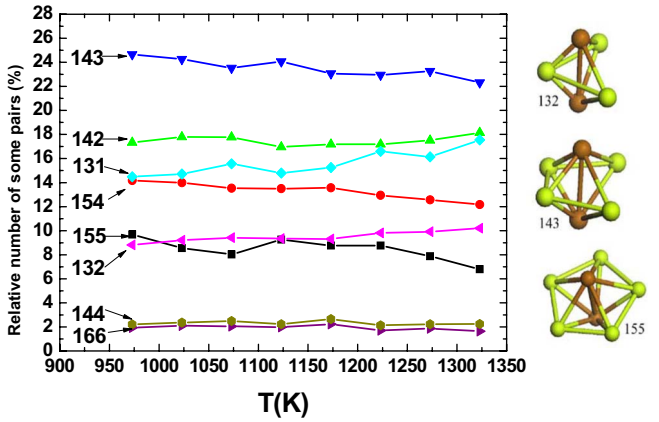

FIG. 4. (Color online) The statistics of the bond-pairs distribution of the liquid $Al_{60}Cu_{40}$ alloy at different temperatures, together with the topologic structures of some representative pair-types (brown balls are root pairs while green ones are near-neighbor atoms).

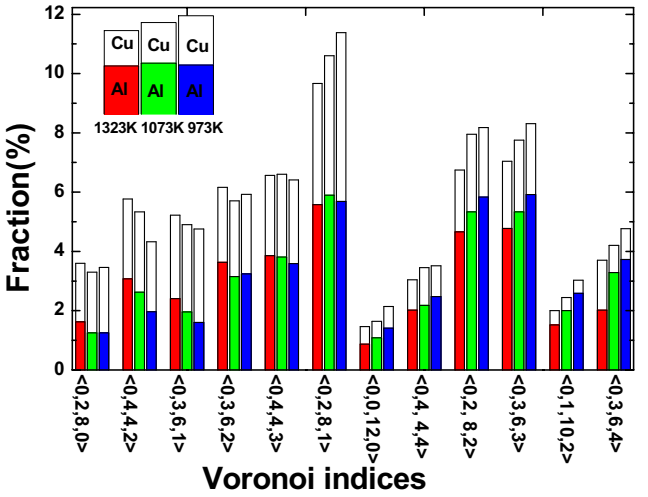

FIG. 5. (Color online) The statistics of the most frequent VC types that appear in the model of the liquid $Al_{60}Cu_{40}$ alloy for three representative temperatures.

are believed to originate from increasing complexity in the polytetrahedral order.[19]

The Honeycutt-Andersen (H-A) index[20] is another useful tool for quantifying the local structures of liquids system. A simplified H-A index[21,22] is characterized by three integers (i j m), which describe, respectively, whether the root pairs of atoms are bonded (i.e., 0 or 1), the number of nearest-neighbor atoms that bond with both of root pairs, and the number of the bonds that connect the nearest-neighbor atoms. In crystals, the fcc and hcp structures are composed of the basic component of 142-type pairs, while the bcc consists of two pair types, 166 and 144. An ideal icosahedron consists of the 155-type pairs, while a distorted icosahedron would also consist of the 154-type and 143-type pairs. Since the first minimum of $g_{\text{Al-Al}}(r)$ is the largest among the first minima of all three kinds of partials, it is employed as the R_{cut} (R_{cut}=3.56 Å) in our H-A index study; note, it changes only a little as a function of temperature (Fig. 2). Figure 4 shows the population of eight H-A indices, together with a schematic drawing of some of these pairs and neighboring atoms. The total population of 155, 154, and 143 pairs for the liquid from the MD simulations constitutes more than 45% of the total pairs, while the total population of 142, 144, and 166 is about 21%. As the temperature is decreased from 1323 to 1223 K, the number of the icosahedral components (143, 154, and 155) increases. Below ~1223 K, little change is observed.

Voronoi tessellation analysis is a more three-dimensional (3D) approach than H-A perspective since it provides a more complete geometrical construction of a central atom to its neighboring atoms.[23,24] In short, the perpendicular bisectors between the central atom and all of its neighboring atoms will form a polyhedron about the central atom and is termed a Voronoi cell (VC), which is quite similar to the well-known Wigner-Seitz cell in crystallography. The total number of the faces of the VC is equivalent to the coordination numbers (CN) for a designated central atom, and the Voronoi index $\langle n_3, n_4, n_5, \ldots \rangle$ is used to differentiate the types of VC, where n_i is the number of i-edged sides of the polyhedron. The clusters in the body-centered-cubic and the face-centered-cubic crystals, for example, have Voronoi indices of $\langle 8,0,0,0 \rangle$ and $\langle 0,12,0,0 \rangle$, respectively, standing for the octahedron and the regular rhombic dodecahedron.

Figure 5 shows the population of the 12 most abundant VC types that appear in liquid $Al_{60}Cu_{40}$ at three representative temperatures. A cutoff distance of R_{cut}=3.56 Å is used in the Voronoi analysis. To improve the statistics, we analyzed each of the 100 atom configurations for the last 2000 steps from the MD calculations, resulting in 200 000 clusters for each temperature. The higher the temperature, the more VC types develop, and well in excess of 340 types were determined. While there are an incredible variety of VC configurations, only a few of them appear with noticeable frequency and the 12 most prevalent VC types constitute 60% of the total cluster population. For instance, the Z11 Kasper polyhedra[20] (some are slightly distorted) with Voronoi indices of $\langle 0,2,8,1 \rangle$, $\langle 0,4,4,3 \rangle$, $\langle 0,3,6,2 \rangle$, and the Z12 of $\langle 0,2,8,2 \rangle$, $\langle 0,3,6,3 \rangle$, $\langle 0,4,4,4 \rangle$, $\langle 0,0,12,0 \rangle$ are the most abundant. The most favored clusters are $\langle 0,2,8,1 \rangle$, followed by $\langle 0,2,8,2 \rangle$, and $\langle 0,3,6,3 \rangle$. The fractions of VCs of $\langle 0,2,8,1 \rangle$, $\langle 0,0,12,0 \rangle$, $\langle 0,4,4,4 \rangle$, $\langle 0,2,8,2 \rangle$, $\langle 0,3,6,3 \rangle$, $\langle 0,1,10,2 \rangle$, and $\langle 0,3,6,4 \rangle$ increase with decreasing the temperature, while the fractions of VCs of $\langle 0,4,4,2 \rangle$, and $\langle 0,3,6,1 \rangle$ decrease with decreasing the temperature. The clusters with coordination number of 10 and 11 (left part of Fig. 5) slightly prefer Cu centers while the clusters with coordination number of 12 and 13 are dominated by Al centers. The most prevalent VCs around Al are $\langle 0,2,8,1 \rangle$, $\langle 0,2,8,2 \rangle$, and $\langle 0,3,6,3 \rangle$, comprising of more than 15% of the whole Voronoi index population and about 2/3 of the $\langle 0,2,8,1 \rangle$, $\langle 0,2,8,2 \rangle$, and $\langle 0,3,6,3 \rangle$ population. The representative topological structures of the most frequent clusters are depicted in Fig. 6, together with their Voronoi cells.

It is interesting to note that the icosahedral cluster $\langle 0,0,12,0 \rangle$ is not the most abundant index, but it is within the top 12 and represents ~1.5% (~1% for Al-centered and 0.5% for Cu-centered) of the entire population. It has been proposed that the stability of a supercooled liquid state is

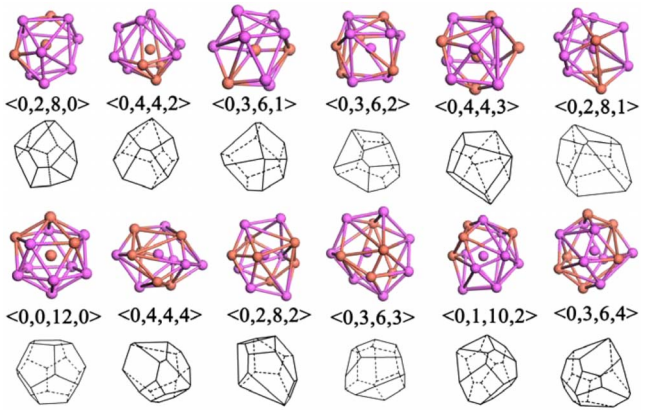

FIG. 6. (Color online) The representative topologic structures of the most frequent clusters (ball and stick) as well as their Voronoi cells (full and dot lines).

strongly correlated with icosahedral local structures.[25–27] It has been further proposed[28–30] that Voronoi polyhedra exhibiting 12 shell atoms and 20 faces such as $\langle 0,2,8,2\rangle$, $\langle 0,3,6,3\rangle$, and $\langle 0,4,4,4\rangle$ may be considered as distorted icosahedral clusters. In order to see in more detail which of the VCs are indeed the distorted icosahedra, we calculated the bond orientation order parameter $\hat{W}_6$ (Ref. 31) for the center atom of each polyhedron using the results of $R_{\mathrm{cut}}=3.56$ Å. The distribution of the $\hat{W}_6$ values for the clusters in the 12 most populous Voronoi indices are shown in Fig. 7. We find that the polyhedrons having the same Voronoi index can have very different $\hat{W}_6$ values. For example, a perfect icosahedral structure, (i.e., equivalent bond angles) is known to have a Voronoi index of $\langle 0,0,12,0\rangle$ and a $\hat{W}_6$ value of −0.169. However, as one can see from Fig. 7, the clusters that have a Voronoi index of $\langle 0,0,12,0\rangle$ do exhibit a much broader distribution of $\hat{W}_6$ values. This indicates that $\hat{W}_6$ values are very sensitive to the angular distortions. Nevertheless, the distribution of the $\hat{W}_6$ values from the $\langle 0,0,12,0\rangle$ type clusters can be seen to be distinct from that of other types of Voronoi polyhedra and are weighted on the negative side (i.e., distributed more toward icosahedral symmetry) of the histogram. From the distributions of $\hat{W}_6$ values shown in Fig. 7, we can see that the proposed icosahedral-like $\langle 0,2,8,2\rangle$, $\langle 0,3,6,3\rangle$, and $\langle 0,4,4,4\rangle$ clusters do not exhibit $\hat{W}_6$ distributions expected for icosahedral symmetry. In other systems such as $Zr_{73}Pt_{27}$ (Ref. 32) $Zr_{35}Cu_{65}$ glasses, $\langle 0,2,8,2\rangle$, and $\langle 0,1,10,2\rangle$ clusters do have $\hat{W}_6$ distribution similar to that of $\langle 0,0,12,0\rangle$ and can be regarded as icosahedral-like clusters.

The local structure analysis using the Voronoi tessellation method also provides us with a convenient way to look into the local chemical ordering the liquid. The chemistry around each atom in the liquid can be determined by counting the shell atoms in each polyhedron obtained by the Voronoi tessellation analysis. The average coordination number for averaging over all atoms is shown in Fig. 8(a). The CN averaged over all atoms decreases slightly from ~11.50 to ~11.26 with increasing temperature from 973 to 1323 K. While the change in the total CN with temperature is small, the ratio between the CNs of the Al-centered and Cu-centered decreases with increasing temperature [Fig. 8(b)]. This strongly suggests that there is a tendency for the bonding between Al-Al and Al-Cu to increase while Cu-Cu bonds decrease with decreasing temperature, indicating increase in chemical ordering as the liquid approaches its melting temperature.

How the clusters of the same CN are distributed as a function of temperature is also important. The distribution of various coordinated-clusters for three temperatures, 973, 1073, and 1323 K, is shown in Fig. 8(c). The liquid is dominated by clusters with CN's of 11 and 12 [Fig. 8(c)]. For the small clusters (CN≤11), the fraction decreases with de-

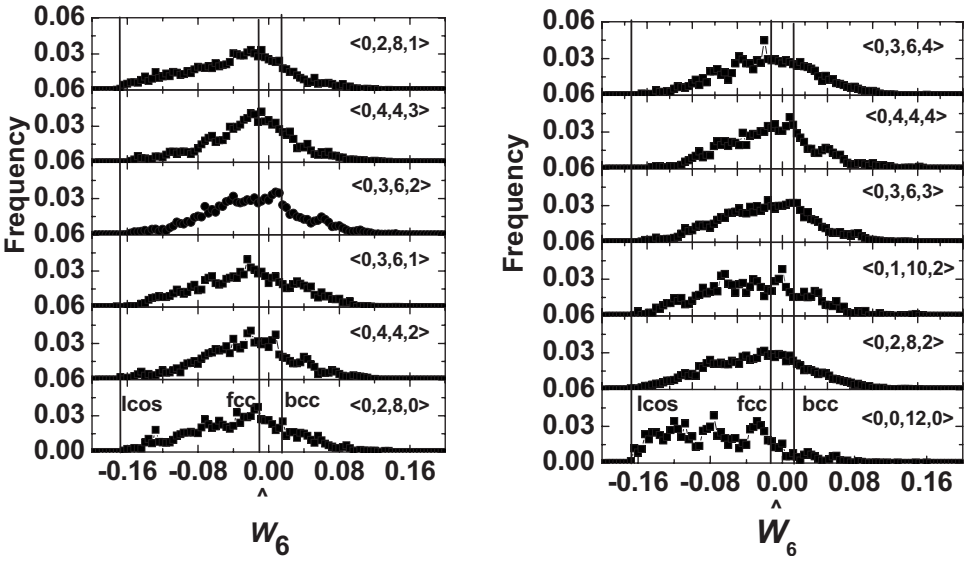

FIG. 7. The calculated frequency density of $\hat{W}_6$ distributions of $Al_{60}Cu_{40}$ at $T=973$ K for 12 types of the most abundant polyhedra from Voronoi indices. The vertical lines indicate the $\hat{W}_6$ values for the ideal icosahedral (−0.169), fcc (−0.013) and bcc (0.013) structures, as indicated on the figure. Note that the $\langle 0,0,12,0\rangle$ barely spans the $\hat{W}_6$ value for an icosahedron.

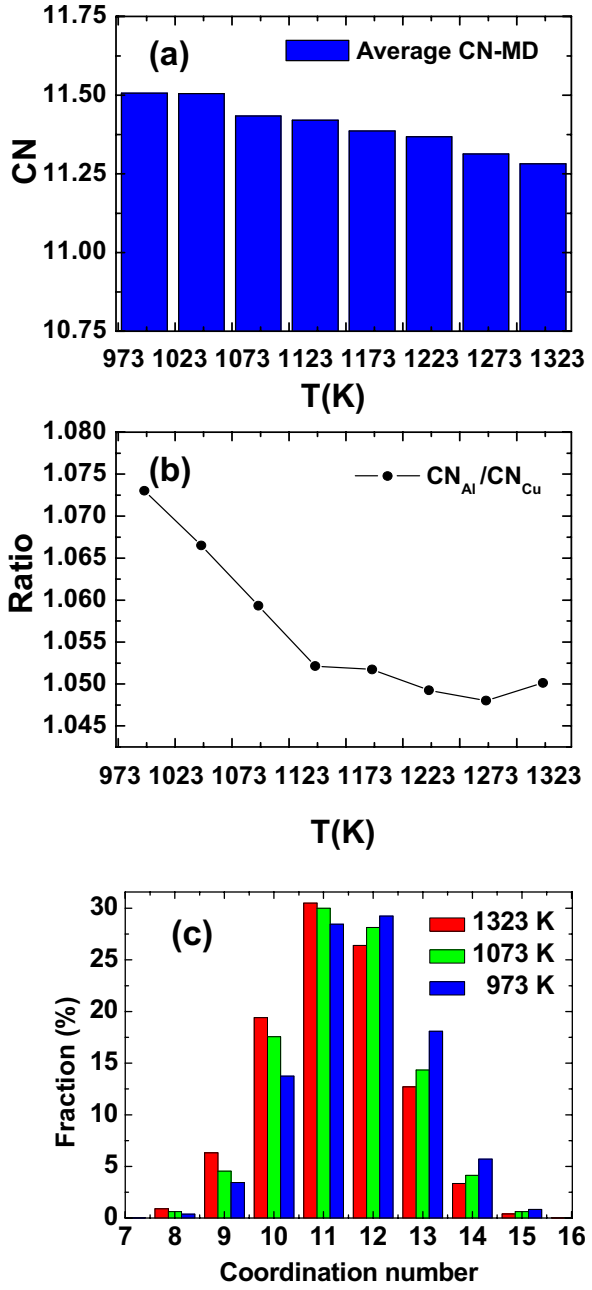

FIG. 8. (Color online) (a) The average coordination number of the liquid $Al_{60}Cu_{40}$ alloy. (b) The ratio between the CNs of the Al-centered and Cu-centered. (c) The distribution of average coordination number at 973, 1073, and 1323 K.

creasing temperatures; for the big clusters (CN≥12), the fraction increases with decreasing temperatures. The relative shift between the population of CN-11 and CN-12 clusters in the liquid as the temperature is changed is consistent with the temperature dependence of the CN, as shown in Fig. 8(a). To demonstrate how the local chemistry changes with temperature more clearly, the CN distributions are separated into the respective Al-centered and Cu-centered while the population of Al and Cu atoms is represented by indexes, (m, n) for Al and Cu, respectively, while the total CN=$m+n$. In Figs. 9(a) and 9(b), the fraction of the all clusters, (m, n) types, for Al-centered and Cu-centered is shown for three representative temperatures. Al-centered clusters prefer 7 Al and 5 Cu neighboring atoms at 1323 K [i.e., (7, 5)]. With decreasing temperature, the population of the (8, 5) type clusters increases and the (7, 5) type clusters decreases. For the Cu centered clusters, the (7, 3) is the most abundant at all temperatures, but the population of the (8, 3) type clusters increases with decreasing the temperature.

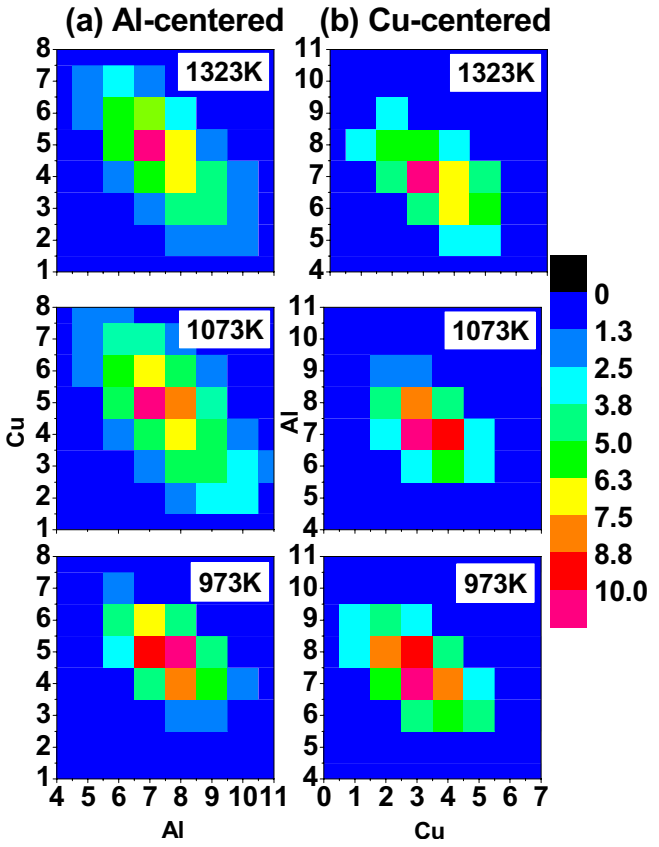

FIG. 9. (Color online) (a) The Al-centered and (b) Cu-centered CN distribution at 973, 1073, and 1323 K.

C. Comparison with metastable crystalline phases

The Al-Cu alloy forms a variety of crystalline phases. As the liquid is cooled below its melting temperature, we would expect that the SRO to tend toward similar structures found in stable or metastable phases near its composition. By comparing the similarities and difference between liquid and crystalline structures, hints to the topological and chemical barriers to nucleation maybe observed. Some typical phases of Al-Cu crystal are listed in the Table I (some unknown or complex phases are ignored).[33,34] A typical cluster of crystals, which usually has more than three shell atoms in a single plane, will meet the "degeneracy" problem when tessellated by the common Voronoi algorithms, but they can still be analyzed manually.[35] For example, the β phase has the body-centered-cubic structure, and both the ε_2 and γ phases belong to the space group of $P6_3/mmc$. They are highly symmetrically packed and show particular Voronoi indices, in contrast, the randomly packed liquid structure can hardly form such regular clusters. Nevertheless, the γ_1 and θ

TABLE I. The crystalline and quasicrystalline phases of the Al-Cu system as well as their corresponding Voronoi indices and fractions in the liquid models (at 973 K).

Symbol	Crystallographic data	Corresponding Voronoi Index	Fraction in our models (%)
η_1	$oP16$, $Pban$		
	$oC16$, $Cmmm$	$\langle 0,4,8,0\rangle$	0
η_2	$mC20$, $C2/m$		
ζ_1	$hP42$, $P6/mmm$		
ζ_2	monoclinic (unknown)		
ε_1	cubic (unknown)		
ε_2	$hP4$, $B8_1$, $P63/mmc$, NiAs type	$\langle 2,0,6,0\rangle$	0.01
δ	rhombohedral, $R3m$, R-type γ-brass		
γ_0	High temperature phase (unknown)		
γ_1	$cP52$, $D8_3$, P-$43m$, P-type, γ-brass	$\langle 0,3,6,0\rangle$, $\langle 3,0,3,3\rangle$	2.12, 0
β_0	High temperature phase (unknown)		
β	$cI2$, $A2$, $Im3m$, W-type	$\langle 0,6,0,8\rangle$	0.004
γ	$D0_{19}$, $P63/mmm$, Cu_3Ti-type	$\langle 0,6,4,2\rangle$	0
α	$D0_{22}$, $I4/mmm$	$\langle 0,8,0,4\rangle$	0
θ	$tI12$, $I4/mcm$	$\langle 0,2,8,0\rangle$	3.46

phases of the Cu-Al alloys have the standard Z9 (the tricapped trigonal prism packing) and Z10 (the bicapped square Archimedean antiprism) Kasper polyhedra with Voronoi indices of $\langle 0,3,6,0\rangle$ and $\langle 0,2,8,0\rangle$, which also exists in a large population in our liquid models. Gaskell[36] discovered that some amorphous alloys have the same type of local structures as their crystalline compounds with similar composition. But we observe no such correlation in the Al-Cu alloy. However, the phase diagram of Al-Cu alloy indicates that the structures of its crystalline phases depend largely on the compositions, so more liquid models that have exactly the same compositions with the corresponding crystalline phases will be investigated in the future work.

D. Dynamical properties

The experimentally validated *ab initio* MD allows for analysis beyond the average structures. Reliable thermodynamic and thermophysical properties are critical for accurate modeling of nucleation and growth, but are difficult to obtain experimentally. For instance, the dynamical properties of the liquid Al-Cu alloy can be studied by calculating the mean-square displacement (MSD) as a function of time using the following:

$$\langle R_\alpha^2(t)\rangle = \frac{1}{N_\alpha}\left\langle \sum_{i=1}^{N_\alpha} |R_{i\alpha}(t+\tau) - R_{i\alpha}(\tau)|^2 \right\rangle, \tag{7}$$

where N_α is the total atomic number of α species, $R_{i\alpha}$ is the coordinates of the atom i, and τ is the arbitrary origin of time. The MSD in the limit of long time should behave linearly with the time step, and the slope of the line is dependent on the self-diffusion constant D defined by the Einstein relationship,

$$D = \lim_{t\to\infty} \langle R_{i\alpha}^2(t)\rangle / 6t. \tag{8}$$

The results show that the atomic MSD maintains good linearity with respect to the time step, indicating the calculated systems are a good approximation of the liquid states. The self-diffusion constants as the functions of temperatures are plotted in Fig. 10. The increase in diffusivity with increasing of the temperatures is as expected since the atoms in the liquid states will increase their motility with increasing temperature. The calculated results of self-diffusion constants are 2.7×10^{-9} and 5.3×10^{-9} m^2/s for Al, and 2.4×10^{-9} and 4.8×10^{-9} m^2/s for Cu, respectively, at the temperatures of 973 and 1323 K. In previous theoretical

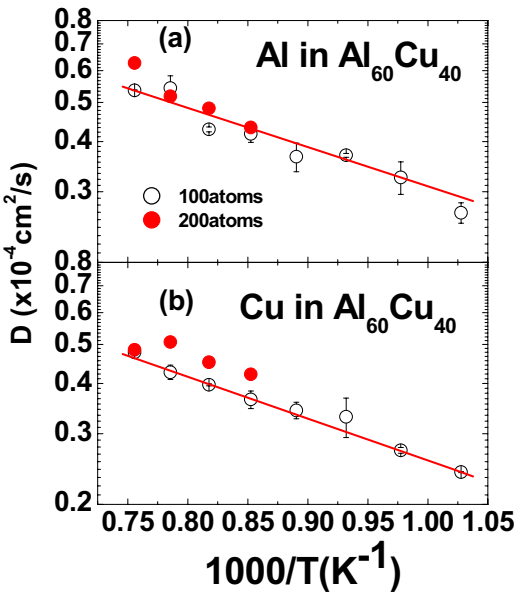

FIG. 10. (Color online) The self-diffusion constant D plotted in logarithmic scale. The red lines are the linearly fitted results. The open and solid circles are from 100-atom and 200-atom simulations, respectively.

literatures, the self-diffusion constants of Al atoms are 5.6×10^{-9} m^2/s at 1000 K in the Al-Si system,[37] 5.2×10^{-9} m^2/s at 1000 K in the pure Al liquid.[38] The diffusion properties of Al atoms in different systems will vary remarkably. The previous experimental data[39,40] show that in the liquid Al-Cu alloys, the self-diffusion constants of Cu will decrease with the increasing concentration of Cu at a designated temperature. The estimated value of self-diffusion constant of Cu atoms in $Al_{60}Cu_{40}$ is about 3.7×10^{-9} m^2/s at 973 K, slightly larger than our calculated results. We notice that the small number of atoms use in our present simulations may cause some errors in the calculation of diffusion constants. As one can see from Fig. 10, the difference between the diffusion constants from the simulations using 100- and 200-atom unit cells can be as large as 10%.

The change in the self-diffusion constants with the temperatures should follow the Arrhenius relationship,

$$D = D_0 e^{-E_\alpha/k_B T}, \tag{9}$$

where E_α is the activation energy, T is the temperature, D_0 is the pre-exponential factor, and k_B is the Boltzmann constant. In the logarithmic scale, $\ln(D)$ should be proportional to $1/T$. In Fig. 10, it is clearly seen that the self-diffusion constants obeys the rule of Eq. (9) within the tolerance of the error bars. In addition, we can yield the E_α and D_0 by linearly fitting the $\ln D$-$1/T$ relation. The activation energy E_α is 20.6 and 19.7 kJ/mol, and the pre-exponential factor D_0 is 3.52×10^{-8} m^2/s and 2.80×10^{-8} m^2/s, for Al and Cu, respectively. The activation energy of Al is larger than Cu, indicating that the bonding of Al and its surrounding atoms are stronger than that of Cu. Reference 36 reported that the E_α value of Cu was 19–21 kJ/mol, which is consistent with our calculated result.

We have also looked into the dynamical property of Voronoi clusters, in addition to the diffusion behavior of the liquid as discussed above. We calculated the average lifetime of the liquid and the lifetimes of each top 12 abundant clusters as the function of temperature. The results are shown in Fig. 11. The cluster lifetime is defined as the number of MD steps during which a center atom keeps its Voronoi index unchanged. The lifetime of total liquid is defined as: $\Sigma_i p(i)t(i)$, where $p(i)$ and $t(i)$ are the population and lifetime of index i, and i runs over all kinds of indices in a liquid sample. The average lifetime of the liquid as shown in Fig. 11(a) reveals the lifetime of the liquid increases as the temperature is decreased as one would expect. It is also interesting to note from Fig. 11(b) that the lifetimes of the top 12 clusters are very similar (around eight steps), although that of the $\langle 0,0,12,0\rangle$ and $\langle 0,2,8,1\rangle$ are slightly higher and that of $\langle 0,4,4,4\rangle$ and $\langle 0,3,6,4\rangle$ are slightly lower. We also noticed that the lifetimes of the clusters exhibit very large variances. For some clusters, their lifetime can vary from a few MD steps to about 100 MD steps during the simulation. Nevertheless, the very short averaged lifetime of the clusters indicates that the clusters are transient entities in the liquid. These results suggest that the dynamics in the liquid seems quite homogeneous and this dynamical homogeneity persists for all the temperatures we studied in this paper. How this dynamical homogeneity may contribute to nucleation in the undercooled liquid will require further study.

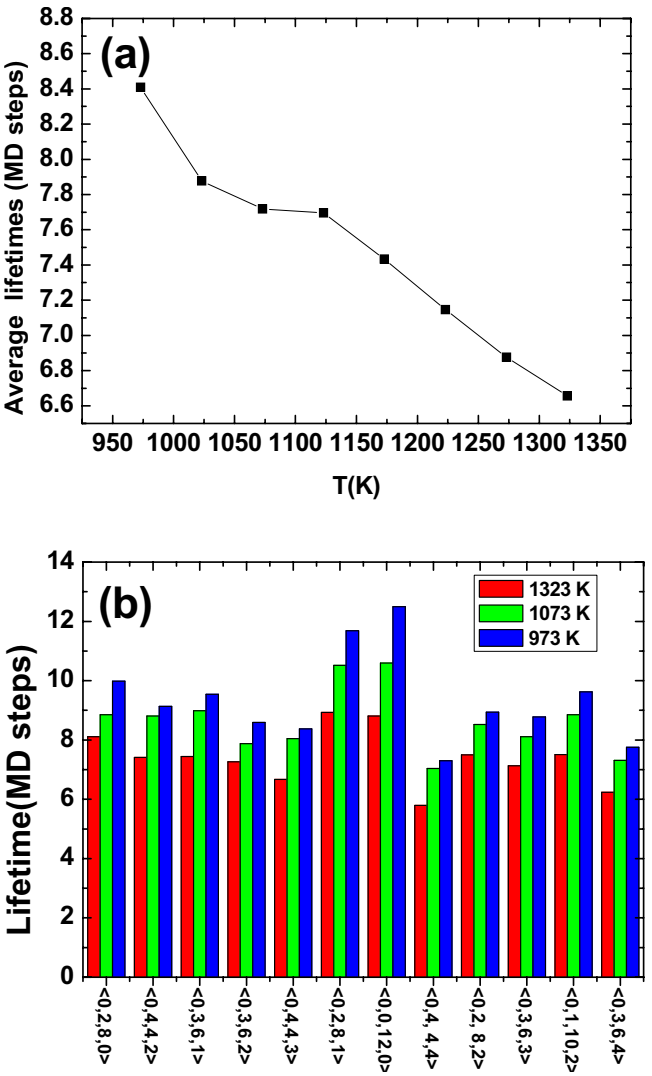

FIG. 11. (Color online) (a) The average lifetimes for all the Voronoi clusters in $Al_{60}Cu_{40}$ at different temperatures; (b) The lifetime for the most frequent VC types that appears in the model of the liquid $Al_{60}Cu_{40}$ alloy for three representative temperatures.

IV. CONCLUSIONS

In summary, the local structures of the liquid $Al_{60}Cu_{40}$ alloy over a 400 K superheat range are shown to be complex. The simulations of the liquid structures are verified by comparing the structure factor and pair-correlation functions with the experimental data and by the investigation of the dynamic properties. Analysis of the models of the liquid $Al_{60}Cu_{40}$, it is found that the coordination numbers of the atoms are mainly between 11 and 12. The topologic analysis of the local structures shows that the chemical environment of the central atoms is highly diversified, and the distorted icosahedra may play an important roll in the structure of the liquid alloys. The local structures of the crystalline phases of the Al-Cu composition show that their structures have no

telltale signatures of the metastable or stable phases.

The analysis of the dynamics of these models shows that the lifetimes of the icosahedral-like clusters increases with decreasing temperature. This suggests that changes in the thermophysical properties of the undercooled liquid, diffusion, viscosity etc., can be attributed to specific topological changes in the liquid atomic structure. More work needs to be done to gain an understanding on how these topological changes affect such properties as atomic mobility and to what extent these changes are mediated by chemistry and simple topology.

ACKNOWLEDGMENTS

One of the authors (S.W.) was supported by the NSF of China (Grant No. 60578046), and the Fudan High-End Computing Center. Ames Laboratory is operated for the U.S. Department of Energy by Iowa State University under Contract No. DE-AC02-07CH11358. This work was supported by the Director for Energy Research, Office of Basic Energy Sciences, including a grant of computer time at the National Energy Research Supercomputing Center (NERSC) in Berkeley. The work at the Advanced Photon Source was supported under Contract No. DE-AC02-06CH11357.

[1] A. L. Greer and E. Ma, MRS Bull. **32**, 611 (2007).
[2] H. W. Sheng, W. K. Luo, F. M. Alamgir, J. M. Bai, and E. Ma, Nature (London) **439**, 419 (2006).
[3] H. W. Sheng, H. Z. Liu, Y. Q. Cheng, J. Wen, P. L. Lee, W. K. Luo, S. D. Shastri, and E. Ma, Nature Mater. **6**, 192 (2007).
[4] T. C. Hufnagel, Nature Mater. **3**, 666 (2004).
[5] L. Margulies, M. J. Kramer, R. W. McCallum, S. Kycia, D. R. Haeffner, J. C. Lang, and A. I. Goldman, Rev. Sci. Instrum. **70**, 3554 (1999).
[6] A. P. Hammersley, S. O. Svensson, M. Hanfland, A. N. Fitch, and D. Häusermann, High Press. Res. **14**, 235 (1996).
[7] Y. Waseda and M. Ohtani, Phys. Status Solidi B **62**, 535 (1974).
[8] T. Egami and S. J. L. Billinge, *Underneath the Bragg Peaks: Structural Analysis of Complex Materials* (Pergamon/Elsevier, London, 2003).
[9] O. J. Eder, E. Erdpresser, B. Kunsch, H. Stiller, and M. Suda, J. Phys. F: Met. Phys. **10**, 183 (1980).
[10] G. Kresse and J. Furthmüller, Comput. Mater. Sci. **6**, 15 (1996).
[11] S. Nosé, J. Chem. Phys. **81**, 511 (1984).
[12] W. G. Hoover, Phys. Rev. A **31**, 1695 (1985).
[13] A. F. Crawley, Int. Metall. Rev. **19**, 32 (1974).
[14] P. A. Egelstaff, *An Introduction to the Liquid State* (Clarendon, Oxford, 1992).
[15] D. Waasmaier and A. Kirfel, Acta Crystallogr., Sect. A: Found. Crystallogr. **51**, 416 (1995).
[16] N. W. Ashcroft and D. C. Langreth, Phys. Rev. **159**, 500 (1967).
[17] A. B. Bhatia and D. E. Thornton, Phys. Rev. B **2**, 3004 (1970).
[18] Y. Waseda, *The Structure of Non-Crystalline Materials* (MacGraw Hill, New York, 1980).
[19] N. Jakse and A. Pasturel, Phys. Rev. Lett. **91**, 195501 (2003).
[20] J. D. Honeycutt and H. C. Andersen, J. Phys. Chem. **91**, 4950 (1987).
[21] C. Fan, P. K. Liaw, V. Haas, J. J. Wall, H. Choo, A. Inoue, and C. T. Liu, Phys. Rev. B **74**, 014205 (2006).
[22] P. Ganesh and M. Widom, Phys. Rev. B **74**, 134205 (2006).
[23] J. L. Finney, Proc. R. Soc. London, Ser. A **319**, 479 (1970).
[24] J. L. Finney, Nature (London) **266**, 309 (1977).
[25] P. J. Steinhardt, D. R. Nelson, and M. Ronchetti, Phys. Rev. Lett. **47**, 1297 (1981).
[26] T. Egami, J. Non-Cryst. Solids **353**, 3666 (2007).
[27] G. W. Lee, A. K. Gangopadhyay, K. F. Kelton, R. W. Hyers, T. J. Rathz, J. R. Rogers, and D. S. Robinson, Phys. Rev. Lett. **93**, 037802 (2004).
[28] L. Yang, S. Yin, X. D. Wang, Q. P. Cao, J. Z. Jiang, K. Saksl, and H. Franz, J. Appl. Phys. **102**, 083512 (2007).
[29] X. D. Wang, S. Yin, Q. P. Cao, J. Z. Jiang, H. Franz, and Z. H. Jin, Appl. Phys. Lett. **92**, 011902 (2008).
[30] T. Fukunaga, K. Itoh, T. M. Otomo, K. M. Sugiyama, H. Kato, M. Hasegawa, A. Hirata, Y. Hirotsu, and A. C. Hannon, Intermetallics **14**, 893 (2006).
[31] P. J. Steinhardt, D. R. Nelson, and M. Ronchetti, Phys. Rev. B **28**, 784 (1983).
[32] S. Y. Wang, C. Z. Wang, M. Z. Li, L. Huang, R. T. Ott, M. J. Kramer, D. J. Sordelet, and K. M. Ho, Phys. Rev. B **78**, 184204 (2008).
[33] G. V. Raynor, *Annotated Equilibrium Diagrams, No. 4* (The Institute of Metals, London, 1944).
[34] P. Villars and L. D. Calbert, *Pearson's Handbook of Crystallographic Data for Intermetallic Phases* (Materials Park, OH, 1985).
[35] C. B. Barber, D. P. Dobkin, and H. Huhdanpaa, ACM Trans. Math. Softw. **22**, 469 (1996).
[36] P. H. Gaskell, Nature (London) **276**, 484 (1978).
[37] M. Ji and X. G. Gong, J. Phys.: Condens. Matter **16**, 2507 (2004).
[38] D. Alfè and M. J. Gillan, Phys. Rev. Lett. **81**, 5161 (1998).
[39] U. Dahlborg, M. Besser, M. Calvo-Dahlborg, S. Janssen, F. Juranyi, M. J. Kramer, J. R. Morris, and D. J. Sordelet, J. Non-Cryst. Solids **353**, 3295 (2007).
[40] Y. Du, Y. A. Chang, B. Y. Huang, W. P. Gong, Z. P. Jin, H. H. Xu, Z. H. Yuan, Y. Liu, and Y. H. He, Mater. Sci. Eng., A **363**, 140 (2003).